AN EMBEDDED DOMAIN TECHNIQUE BASED ON LEVEL-SETS FOR FINITE ELEMENT METHOD (FEM) FLUID-SHELL COUPLING

Rodolfo A. K. Sanches and Humberto B. Coda

Departamento de Engenharia de Estruturas, Escola de Engenharia de São Carlos, Universidade de São Paulo, São Carlos, SP, Brasil, raks@sc.usp.br, http://www.set.eesc.usp.br

Keywords: positional fem, geometrically nonlinear shell, fluid-structure interaction, inflatable structures, immersed boundary.

Abstract.

This paper presents a robust level-set-based approach that integrates a Lagrangian shell finite element solver and an Eulerian finite element high speed fluid flow solver, with no need for mesh adaptation, where the fluid representation relies on a fixed unstructured mesh larger or equal to the initial fluid domain. The Eulerian fluid solver is based on a fully explicit scheme, with time integration based on characteristics over an unstructured mesh of four nodes tetrahedral finite elements. The structure is modeled using a positional finite element method formulation to deal with geometrical nonlinear dynamics of shells based on the minimum potential energy theorem written regarding nodal positions and generalized unconstrained vectors, not displacements and rotations, avoiding the use of large rotation approximations. The fluid-shell interface inside the fluid mesh is tracked with level sets of a boundary signed distance function. The conservation laws and continuity at the interface are enforced by applying proper interface boundary conditions to the fluid and shell solvers at the beginning of each time step. For the fluid case this is done by enforcing values over the nodes outside the domain which are connected to nodes inside, together with a signed distance based slope limiter that also changes velocities values on inside nodes settled very close to the boundary avoiding stability problems when most of the element volume is outside the structural region.

1 INTRODUCTION

The mathematical model for physics problems is traditionally done in a Lagrangian or Eulerian description. The Lagrangian description expresses the continuum medium movement in terms of the initial configuration and time, being very efficient for problems where finite displacements are the main variables, such as in solid mechanics. By other hand, the Eulerian description is defined in terms of final configuration and time, being well used for problems where the variables are velocities instead of displacements, such as for fluid mechanics (Valiappan, 1981).

Both fluid and solid mechanics are involved in the study of fluid-structure interaction problems, implying the need to couple Eulerian description to Lagrangian description. One widely used way to deal with such situations is to solve the solid based on a Lagrangian description and the fluid based on an Arbitrary Lagrangian-Eulerian (ALE) description, in which an arbitrary velocity may be applied to the reference domain.

Using ALE description for Navier-Stokes equations together with some mesh moving technique is a methodology able to deal with many fluid-structure interaction problems (Soria and Casadei, 1997; Donea et al., 1982; Teixeira and Awruch, 2005; Sanches and Coda, 2008). However, some problems of large scale of displacements, such as air-bag or parachute deployment, will require also a re-mesh technique if the ALE description is employed.

Some authors have proposed immersed methods for Eulerian-Lagrangian coupling, most of them in the finite difference context, considering immersed boundary in a structured mesh (Cirak and Radovitzky, 2005; Habbal, 2009; M. Arienti and Shepherd, 2008).

The technique proposed here couples a Lagrangian shell finite element solver to an Eulerian fluid finite element solver by considering the shell boundary moving inside the fluid unstructured mesh in which it is immersed. The shell position is tracked with level sets of a boundary signed distance function, and the fluid Dirichlet boundary conditions are applied by enforcing a ghost flow over the nodes immediately outside the shell boundary and at same time limiting the velocity slope based on the signed distance function.

The outline of the paper consists in first describe shell and fluid formulations, then describe the coupling algorithm, and finally present examples of inflatable structure problems giving a qualitative demonstration of feasibility and quality of the proposed technique.

2 FINITE ELEMENT METHOD FOR FLUID MECHANICS

The Eulerian description of fluid dynamics governing equations (Navier-Stokes) is well known, leading to the equations:

$$\frac{\partial \rho}{\partial t} = -\frac{\partial(\rho u_i)}{\partial x_i}, \tag{1}$$

which is the mass conservation equation,

$$\frac{\partial(\rho u_i)}{\partial t} = -\frac{\partial(u_j \rho u_i)}{\partial x_j} + \frac{\partial \tau_{ij}}{\partial x_j} - \frac{\partial p}{\partial x_i} + \rho g_i, \tag{2}$$

which is the momentum equation, and

$$\frac{\partial(\rho E)}{\partial t} = -\frac{\partial}{\partial x_j}(u_j \rho E) + \frac{\partial}{\partial x_i}\left(k\frac{\partial T}{\partial x_i}\right) - \frac{\partial}{\partial x_j}(u_j p) + \frac{\partial}{\partial x_j}(\tau_{ij} u_j) + \rho g_i u_i, \tag{3}$$

which is the energy equation. In these equations ρ is the specific mass, u_i is the i velocity component, with i being the Cartesian axis 1, 2 or 3 (x, y or z), p is the pressure, τ_{ij} are the

deviatoric stress tensor (i, j) components, g_i is the i direction field forces constant, E is the specific energy, T is the temperature ans k is the thermal conductivity.

2.1 Time integration along characteristics

Characteristics are the curves that indicate the spatial positions by where a given property ϕ is transported (Fortuna, 2000) (see Fig 1).
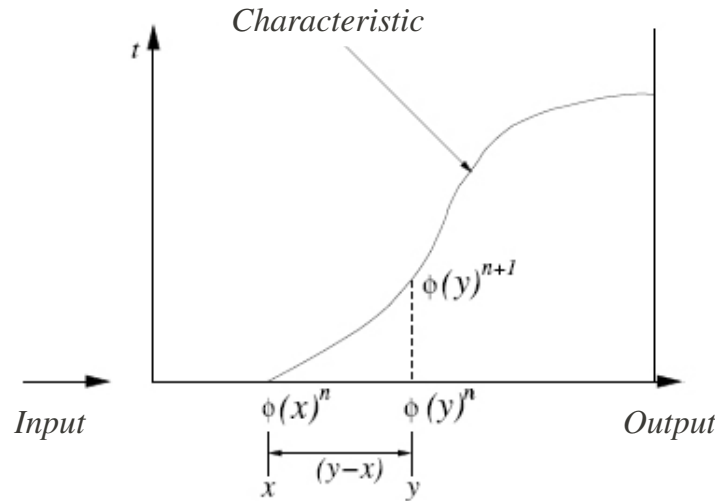

Figure 1: Characteristics for non-linear convection

If there is no diffusion, the time variation of ϕ over a characteristic of coordinates x' is by definition null:

$$\frac{d\phi}{dt}(x', t) = 0. \tag{4}$$

For the Navier-Stokes equations we can write:

$$\frac{\partial \phi(x', t)}{\partial t} - Q(x') = 0, \tag{5}$$

where $Q(x')$ contains all the non convective terms.

We assume the following approximation for Eq. (5) (Zienkiewicz and Taylor, 2000):

$$\frac{\phi(y)_{n+1} - \phi(x)_n}{\Delta t} \approx \theta(Q(y)_{n+1}) + (1 - \theta)(Q(x)_n), \tag{6}$$

where x and y means respectively the characteristic positions at $t = n$ and $t = n + 1$, θ is a constant with value 0 for explicit solution and may be chosen larger than zero 0 and smaller than 1 for semi-implicit or implicit solution.

The product $u\phi$ and the term $Q(x)$ may be approximated by Taylor resulting the following expressions:

$$u\phi(x)_n = u\phi(y)_n - (y - x)\frac{\partial (u\phi(y))_n}{\partial x} + \frac{(y - x)^2}{2}\frac{\partial^2 (u\phi(y)_n)}{\partial x^2} + O(\Delta t^3), \tag{7}$$

$$Q(x)_n = Q(y)_n - (y - x)\frac{\partial Q(y)_n}{\partial x} + O(\Delta t^2). \tag{8}$$

Dividing Eq. (7) by u and substituting on Eq. (6), then substituting $Q(x)_n$ by Eq. (8) and assuming $\theta = 0$ (explicit form), results:

$$\frac{1}{\Delta t}\left(\phi(y)_{n+1} - \phi(y)_n + \frac{(y-x)}{u}\frac{\partial(u\phi(y))_n}{\partial x} - \frac{(y-x)^2}{2u}\frac{\partial^2(u\phi(y)_n)}{\partial x^2}\right) =$$
$$Q(y)_n - (y-x)\frac{\partial Q(y)_n}{\partial x} + O(\Delta t^2). \tag{9}$$

Assuming $\Delta t = (y - x)/u$ on Eq. (9) and reorganizing, we have:

$$\phi(y)_{n+1} = \phi(y)_n - \Delta t\left(\frac{\partial(u\phi(y))_n}{\partial x} - Q(y)_n\right)$$
$$+\frac{(\Delta t)^2}{2}u\frac{\partial}{\partial x}\left(\frac{\partial(u\phi(y)_n)}{\partial x} - Q(y)_n\right) + O(\Delta t^2). \tag{10}$$

One important point about this procedure is that the high order terms of Eq. (10), obtained due to time integration along characteristics, introduce dissipation on stream lines direction, which as shown by Zienkiewicz and Taylor (2000) are equivalent to the SUPG schemes when the time interval tends to the critical time interval, and gets smaller effects as the time interval get smaller.

2.1.1 Navier-Stokes equations discretization

From the same procedure that produced Eq. (10), applied to Eq. (2), one may write:

$$\Delta(\rho u_i)_{n+1} = \Delta t\left(-\frac{\partial(u_j\rho u_i)}{\partial x_j} + \frac{\partial \tau_{ij}}{\partial x_j} - \frac{\partial p}{\partial x_i} + \rho g_i\right)_n +$$
$$\frac{\Delta t^2}{2}\left(u_k\frac{\partial}{\partial x_k}\left(\frac{\partial(u_j\rho u_i)}{\partial x_j} - \frac{\partial \tau_{ij}}{\partial x_j} + \frac{\partial p}{\partial x_i} - \rho g_i\right)\right)_n, \tag{11}$$

where all the right hand side terms are known at the instant $t = n$.

Based on the Eulerian mass conservation equation, Zienkiewicz and Taylor (2000) suggest the following expression for explicit solution:

$$\Delta\rho_{n+1} = -\Delta t\frac{\partial(\rho u_i)_{n+\theta}}{\partial x_i} = -\Delta t\left(\frac{\partial}{\partial x_i}(\rho u_i)_n + \theta\frac{\partial(\Delta(\rho u_i))_{n+1}}{\partial x_i}\right), \tag{12}$$

where θ is a arbitrary constant with value between 0.5 and 1.

Finally, applying to Eq. (3) the same procedure that produced (11), we have:

$$\Delta(\rho E)_{n+1} = \Delta t\left(-\frac{\partial(u_i\rho E)}{\partial x_i} + \frac{\partial}{\partial x_i}\left(k\frac{\partial T}{\partial x_i}\right) - \frac{\partial(u_i p)}{\partial x_i} + \frac{\partial(\tau_{ij}u_j)}{\partial x_i} - \rho g_i u_i\right) +$$
$$\frac{\Delta t^2}{2}u_k\frac{\partial}{\partial x_k}\left(\frac{\partial(u_i\rho E)}{\partial x_i}\right) +$$
$$\frac{\Delta t^2}{2}u_k\frac{\partial}{\partial x_k}\left(-\frac{\partial}{\partial x_i}\left(k\frac{\partial T}{\partial x_i}\right) + \frac{\partial(u_i p)}{\partial x_i} - \frac{\partial(\tau_{ij}u_j)}{\partial x_i} + \rho g_i u_i\right)_n. \tag{13}$$

2.2 FINITE ELEMENT discretization

Applying the Galerkin method to Eq. (11), (12) and (13), in order to obtain the spatial discretization, making use of divergence theorem and neglecting the boundary high order terms, we get the following expressions:

$$\int_{\Omega} N\Delta(\rho u_i)d\Omega = \Delta t \int_{\Omega} N \left(-\frac{\partial(u_j\rho u_i)}{\partial x_j} + \rho g_i \right) d\Omega$$
$$-\Delta t \left(\int_{\Omega} \frac{\partial N}{\partial x_j}(\tau_{ij} - \delta_{ij}p)d\Omega + \int_{\Gamma} N(\tau_{ij}n_j - pn_i)d\Gamma \right), \tag{14}$$
$$-\frac{\Delta t^2}{2} \int_{\Omega} \frac{\partial(Nu_k)}{\partial x_k} \left(\frac{\partial}{\partial x_j}(u_j\rho u_i) - \frac{\partial \tau_{ij}}{\partial x_j} + \frac{\partial p}{\partial x_i} - \rho g_i \right) d\Omega$$

$$\int_{\Omega} N\Delta\rho d\Omega = -\Delta t \int_{\Omega} N \left(\rho u_i + \theta\Delta(\rho u_i) \right) \tag{15}$$

and

$$\int_{\Omega} N\Delta(\rho E)d\Omega = \Delta t \int_{\Omega} N \left(-\frac{\partial(u_i(\rho E + p))}{\partial x_i} \right) d\Omega -$$
$$\Delta t \int_{\Omega} \frac{\partial N}{\partial x_i} \left(\tau_{ij}u_j + k\frac{\partial T}{\partial x_i} \right) d\Omega + \frac{\Delta t^2}{2} \int_{\Omega} \frac{\partial(u_j N)}{\partial x_j} \left(\frac{\partial(-u_i(\rho E + p))}{\partial x_i} \right) d\Omega + \tag{16}$$
$$\Delta t \int_{\Gamma} \phi \left(\tau_{ij}u_j + k\frac{\partial T}{\partial x_i} \right) n_i d\Gamma,$$

where N is the shape functions vector.

Writing in a matrix form we have:

$$M\overline{\rho u_i} = \Delta t f_u, \tag{17}$$

$$M\overline{\Delta\rho} = \Delta t f_\rho \tag{18}$$

and

$$M\Delta\overline{\rho E} = \Delta t f_e \tag{19}$$

where f_u, f_ρ and f_e are the right hand side vectors and M is the mass matrix given by:

$$M = \int_{\Omega} \mathrm{N}^T \mathrm{N} d\Omega, \tag{20}$$

The mass matrix M may be easily lumped, which is highly desirable for explicit methods. However the use of consistent mass matrix can prevent spurious variations when Δt is small, as presented by Zienkiewicz and Taylor (2000).

Therefore, we employ the iterative approach to solve the systems based on mass balance given by:

$$(\Delta\phi)_l = (\Delta\phi)_{l-1} + M_L^{-1} \left[B - M(\Delta\phi)_{l-1} \right], \tag{21}$$

where $\Delta\phi$ is the unknowns vector, l is the interaction step, M_L is the lumped matrix, M is the consistent mass matrix and B is the right hand side vector. This procedure converges very fast to the consistent solution for $\Delta\phi$.

Solving Eqs. (17),(18),and (17), all the variables can be computed on instant t_{n+1} based on the thermodynamic equations.

2.3   Shock capturing

We still need to choose a shock capturing technique, as the standard Galerkin method is unable to deal with strong discontinuities, such as shock waves.

Therefore we add an artificial dissipative term based on the pressure second derivative, given by the following expression (Nithiarasu et al., 2006):

$$f_{\mu_a} = \Delta t \mu_a \frac{\partial}{\partial x_i} \left(\frac{\partial \phi}{\partial x_i} \right), \tag{22}$$

where ϕ is the variable to be smoothed and μ_a is the artificial viscosity given by:

$$\mu_a = q_{dif} h^3 \frac{(|\mathrm{u}| + c)}{p_{med}} \left| \frac{\partial}{\partial x_i} \left(\frac{\partial p}{\partial x_i} \right) \right|_e, \tag{23}$$

where $|\mathrm{u}|$ is the modulus of the velocity vector, p_{med} is the pressure average over the element, q_{dif} is an user coefficient taken between 0 and 2, c is the sound speed and h is the element size.

3   POSITIONAL FEM FOR GEOMETRICAL NONLINEAR DYNAMICS OF SHELLS

The methodology employed is based on the minimum potential energy theorem written regarding nodal positions and generalized unconstrained vectors instead of displacements and rotations. This characteristic avoid the use of large rotation approximations The shell formulation is total Lagrangian and, due to its unconstrained vector mapping, it presents constant mass matrix and therefore it is possible to apply the Newmak β integrator as a momentum conserving algorithm.

3.1   Strain measure and specific strain energy potential

We employ the Green strain tensor to derive the proposed formulation. The Green strain tensor is derived directly from the gradient of the configuration change function as depicted on Fig. 2, represented by letter A, given as follows:

$$A_{ij} = \frac{\partial \chi_i}{\partial X_j} \tag{24}$$

where χ is the configuration change function, and X represents variation regarding initial position.

Following Ogden (1984), the Green strain tensor can be written as:

$$E_{ij} = \frac{1}{2} \left[A_{ki} A_{kj} - \delta_{ij} \right] = \frac{1}{2} \left[C_{ij} - \delta_{ij} \right] \tag{25}$$

The variables C_{ij} and δ_{ij} are the right Cauchy-Green stretch tensor and the Kroenecker delta, respectively. The following quadratic strain energy per unit of initial volume is adopted,

$$u_e = \frac{1}{2} E_{ij} C_{ijkl} E_{kl} \tag{26}$$

resulting into a linear elastic constitutive law relating second Piola-Kirchhoff stress and Green strain, usually called Saint-Venant–Kirchhoff elastic law, i.e.:

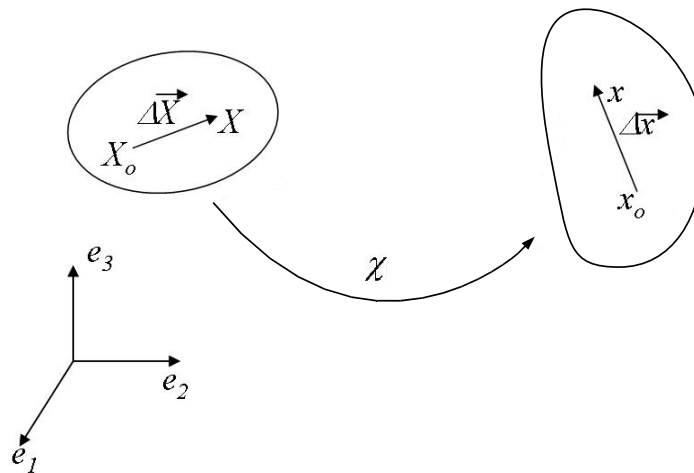$$S_{ij} = \frac{\partial u_e}{\partial E_{ij}} = C_{ijkl} E_{kl} \tag{27}$$

Figure 2: Change of configuration

The elastic tensor is given by

$$C_{ijkl} = \frac{2G\nu}{1 - 2\nu}\delta_{ij}\delta_{kl} + G(\delta_{ik}\delta_{jl} + \delta_{il}\delta_{jk}) \tag{28}$$

Where G is the shear modulus.

The true stress (Cauchy stress) is achieved directly from the Second Piolla-Kirchhoff stress following simple expressions given by Ogden (1984), for instance.

3.2 Positional shell formulation

Shell structures consists on solids with one dimension much larger than the others. Therefore Coda and Paccola (2009) develop the shell formulation based on the middle surface configuration change as depicted on Fig. (3).

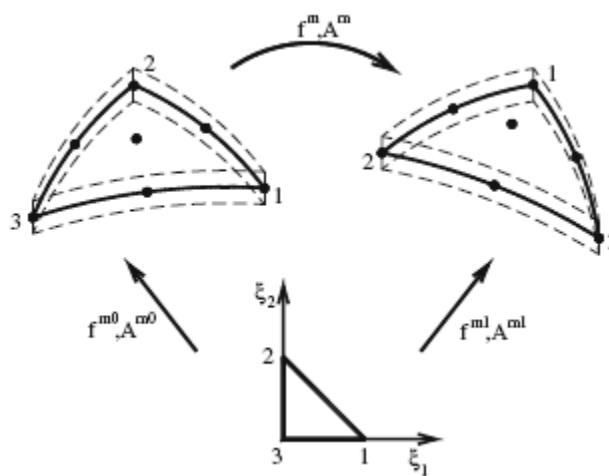Figure 3: Middle surface mapping

The fictitious configuration change functions f^{m0} and f^{m1}, from an auxiliary non-dimensional

space respectively to the initial and final configurations may be written as follows:

$$f_i^{m0} = X_i^m(\xi_1, \xi_2, X_{ji}) = N_j(\xi_1, \xi_2) X_{ji}^m \tag{29}$$

e

$$f_i^{m1} = x_i^m(\xi_1, \xi_2, x_{ji}) = N_j(\xi_1, \xi_2) x_{ji}^m, \tag{30}$$

For any point out of the middle surface, its position at initial and final configuration may be written as:

$$X_i = X_i^m + g_i^0, \tag{31}$$

and

$$x_i = x_i^m + g_i^1, \tag{32}$$

where the g^0 and g^1 are called generalized position vectors for the initial and final configurations.

Considering a linear strain rate along the thickness, the vectors g^0 and g^1 may be written as (Coda and Paccola, 2009):

$$g_i^0 = \frac{h_0}{2} \xi_3 N_j(\xi_1, \xi_2) e_{ij}^0 \tag{33}$$

and

$$g_i^1 = \frac{h_0}{2} \left[\xi_3 + a(\xi_1, \xi_2)\xi_3^2 \right] N_j(\xi_1, \xi_2) \bar{G}_{ij} \tag{34}$$

where $\bar{G}_{ij}$ are the nodal values (unknowns) for the generalized vector at node j at final configuration, h^0 and h are respectively the initial thickness and final thickness, e_i^0 and e_i^1 and the i components for unitary vectors $\overrightarrow{e^0}$ and $\overrightarrow{e^1}$, normal to the midle surface at initial and final configuration and a is the strain rate along thickness.(see Fig. 4).

Finally, the real middle surface configuration change from initial to final configurations is represented by:

$$\overrightarrow{f}^m = \overrightarrow{f}^m \left(\overrightarrow{X}^m \right) = \left(\overrightarrow{f^{m1}} \right) \circ \left(\overrightarrow{f^{m0}} \right)^{-1} \tag{35}$$

The gradient A^m of the configuration change function may be expressed by:

$$A^m = Grad\left(\overrightarrow{f}^m \right) = \frac{\partial \overrightarrow{f}^m}{\partial \overrightarrow{X}^m} = \left(A^{m1} \right) \left(A^{m0} \right)^{-1}. \tag{36}$$

Using the shape functions, one may write A^{m0} and A^{m1} as:

$$A_{ij}^{m0} = f_{i,j}^{m0} = N_{k,j}(\xi_1, \xi_2, \xi_3) X_{ki}, \tag{37}$$

and

$$A_{ij}^{m1} = f_{i,j}^{m1} = N_{k,j}(\xi_1, \xi_2, \xi_3) x_{ki}, \tag{38}$$

where the indexes $,j$ indicate derivatives on direction j.

After evaluating the gradient A, the Green strain tensor and the specific strain energy may be obtained from Eqs. (25) and (26).

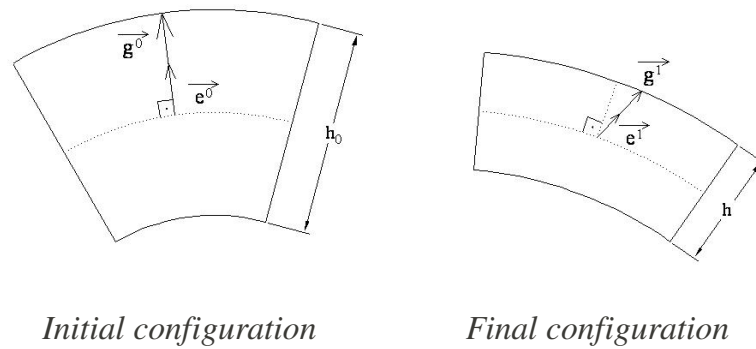*Initial configuration*   *Final configuration*

Figure 4: Generalized vectors

3.2.1 The adopted shell element

The finite element adopted in for this paper is an isoparametric triangular element with 10 nodes (cubic shape functions). Each node has 7 nodal parameters: 3 position vector components x_i with $i = 1, 2$ or 3, 3 components of the generalized position vector $\bar{G}_i$ with $i = 1, 2$ or 3 and the strain ratio along thickness a.

3.3 Time integration

The time integrator employed is the Newmark β, which is summarized as:

$$x_{S+1} = x_S + \Delta t \dot{x}_S + \Delta t^2 \left[\left(\frac{1}{2} - \beta \right) \ddot{x}_S + \beta \ddot{x}_{S+1} \right] \tag{39}$$

and

$$\dot{x}_{S+1} = \dot{x}_S + \Delta t \left(1 - \gamma \right) \ddot{x}_S + \gamma \Delta t \ddot{x}_{S+1}. \tag{40}$$

Coda and Paccola (2009) proved that for a positional total Lagrangian description, the Newmark β with $\gamma = 1/2$ presents momentum and energy conservative properties for most of shell dynamics problems.

3.4 Newton-Raphson procedure

From preceding developments, one may write the equilibrium equation as the minimization of the energy functional as:

$$\frac{\partial U_e}{\partial x} - F + M\ddot{x} + C\dot{x} = 0, \tag{41}$$

where F is the external forces vector, C is the dissipative matrix and M is the mass matrix.

At instant t_{S+1}, the equilibrium is expressed by the following equation:

$$\left. \frac{\partial \Pi}{\partial x} \right|_{S+1} = \left. \frac{\partial U_e}{\partial x} \right|_{S+1} - F_{S+1} + M\ddot{x}_{S+1} + C\dot{x}_{S+1} = 0. \tag{42}$$

From Newmark β method, Eq. (39) and Eq. (40), the equation Eq. (42) becomes:

$$f(x_{S+1}) = \left.\frac{\partial \Pi}{\partial x}\right|_{S+1}$$

$$= \left.\frac{\partial U_e}{\partial x}\right|_{S+1} - F_{S+1} + \frac{M}{\beta \Delta t^2} x_{S+1} - MQ_S + CR_S + \frac{\gamma C}{\beta \Delta t} x_{S+1} - \gamma \Delta t C Q_S = 0, \tag{43}$$

where the vectors Q_s and R_s represent the dynamic contribution from the past and are expressed by:

$$Q_S = \frac{x_S}{\beta \Delta t^2} + \frac{\dot{x}_S}{\beta \Delta t} + \left(\frac{1}{2\beta} - 1\right)\ddot{x}_S \tag{44}$$

and

$$R_S = \dot{x}_S + \Delta t (1 - \gamma)\ddot{x}_S. \tag{45}$$

The second energy functional variation is expressed by:

$$\left.\frac{\partial^2 \Pi}{\partial x^2}\right|_{S+1} = \nabla f(x_{s+1}) = \left.\frac{\partial^2 U_e}{\partial x^2}\right|_{S+1} + \frac{M}{\beta \Delta t^2} + \frac{\gamma C}{\beta \Delta t}. \tag{46}$$

An Taylor series first order approximation for the energy functional f gives:

$$0 = f(x) \cong f(x^0) + \nabla f(x^0)\Delta x. \tag{47}$$

The Newton-Raphson process for each time step is summarized on estimate a value x_{s+1}^0 for the final position x_{s+1}, and apply the interactive process:

$$\nabla f(x_s^l)\Delta x = -f(x_s^l) \tag{48}$$

$$x_{S+1}^{l+1} = x^l + \Delta x, \tag{49}$$

where l is the interactions number. The interactions are interrupted when the admissible error prescribed is reached.

4 FLUID-STRUCTURE COUPLING PROCEDURE

4.1 Implicit boundary representation

Before moving on to the discussion of the immersed boundary conditions prescription, we first elaborate on the representation of the physical domain immersed on an unstructured mesh. The proposed method for enforcing boundary conditions requires to identify all the fluid elements close to the boundary Γ_s and if they are inside or outside the physical domain Ω_f. To this end, a computationally efficient and scalable approach is to use a signed distance function (or, level set function):

$$\phi(x, \Gamma) = \begin{cases} \text{distance}(x, \Gamma) & \text{if } x \in \Omega \\ 0 & \text{if } x \in \Gamma \\ -\text{distance}(x, \Gamma) & \text{otherwise} \end{cases} \tag{50}$$

A discrete representation of the signed distance function can be obtained by combining the fluid shape functions with the signed distance values at the nodes ϕ_I

$$\phi = \sum N_{I,n}\phi_I \tag{51}$$

Note that the shape functions $N_{I,n}$ do not need to conform to the physical boundary since they are only used for interpolation of a scalar field ϕ.

The resulting signed distance function describes after combining several entities again a signed distance function, whose zero level set determines the resulting body shape.

In contrast to the usual parametric mesh based boundary representations (using segments or facets), level set based representations are more suitable for problems with large deformations and topology changes. There are efficient and scalable algorithms for converting a mesh based representation into an implicit representation (e.g., closest point transform).

The interpolated boundary consists of the trace of the signed distance interpolated by linear shape functions on a tetrahedral mesh (the adopted fluid mesh).

Next, all the fluid elements are tagged as *physical*, *fictitious* or *boundary* depending on their position with respect to the physical domain. This classification is performed by computing for each fluid element Ω_{ef} the minimum and maximum signed distance $\min \phi(\Omega_{ef})$ and $\max \phi(\Omega_{ef})$, respectively, then the classification is applied as (see Fig. 5):

- physical element: $\min \phi(\Omega_e) > 0$

- fictitious element: $\max \phi(\Omega_e) \leq 0$

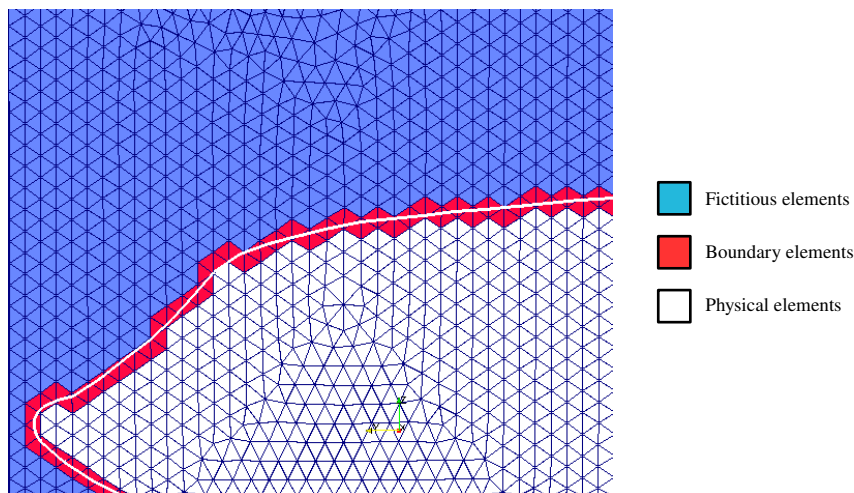- boundary element: neither a physical nor a fictitious element

Figure 5: Elements tags

This classification is unique as it is based on the signed distance function and not on the parametric representation of the physical domain (e.g., via a surface mesh). The purpose of the elements tags is to identify where the nodal fluid parameters must be modified in order to enforce the Dirichlet proper boundary conditions. To this purpose, all the fluid mesh nodes are tagged as *active* or *inactive*. A node k is active if $\phi(k) > 0$ or if k bellows to some boundary fluid element, and inactive otherwise.

This tags are computed for each time step and the inactive nodes as well as the fictitious elements are deactivated from the analysis.

4.2   Fluid Dirichlet boundary conditions

For each fluid node k, we find the closest point l on shell mesh, and store the shell element Ω_{se} for which $l \in \Omega_{se}$ and the non-dimensional shell coordinates (ξ_1, ξ_2) for point l.

The active nodes k outside the physical domain $(\phi(k) < 0)$, need to be populated. For this purpose we project the point k to the closest physical element determining a new point m from where the values of density, specific energy and momentum are linearly extrapolated.

A way to prescribe the velocity at the boundary position would be to change the velocity nodal values of the active nodes k with $\phi(k) < 0$ (ghost nodes) in order to modify the values over the boundary. However this procedure may imply on very large velocity values as $\phi(k)$ becomes close to the element size.

To avoid this problem, we modify the velocity nodal values for the active nodes outside the boundary and also the velocity nodal inside a strip of width δ according to the following equation if the flow is inviscid:

$$\mathbf{u}_f = \mathbf{u}_f + (1 - \frac{\phi}{\delta})[(\mathbf{u}_s - \mathbf{u}_f) \cdot \mathbf{n}]\mathbf{n}. \tag{52}$$

or if the flow is viscous:

$$\mathbf{u}_f = \mathbf{u}_f + (1 - \frac{\phi}{\delta})[\mathbf{u}_s - \mathbf{u}_f] \tag{53}$$

where $\mathbf{u}_f$ is the fluid nodal fluid velocity vector, $\mathbf{u}_s$ is the shell velocity vector evaluated at the shell closest point to the fluid node. This procedure applied to a 1D example is depicted on Fig. 6.
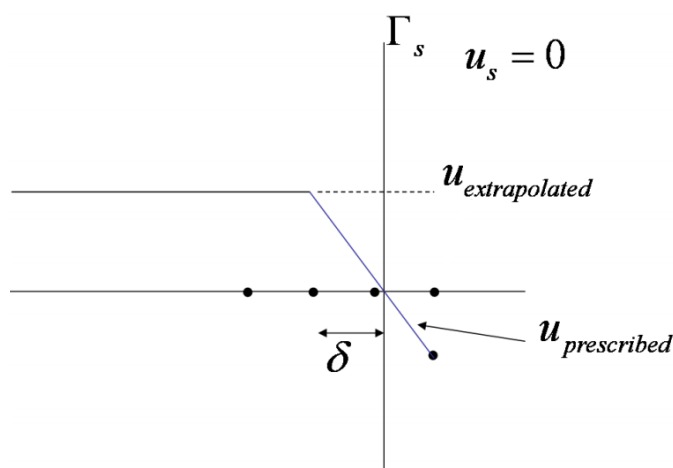

Figure 6: Immersed boundary condition enforcement

The term $(1 - \frac{\phi}{\delta})$ limits the slope of velocity on direction normal to the boundary but also introduces an artificial stiffness to the problem. However if we adopt a δ equal to the element size, this artificial stiffness is equal to the one naturally produced by an mesh of same elements size adapted to the boundary.

4.3 Shell Neumman boundary conditions

Taking advantage of the fluid shape functions, the stress tensor may be evaluated directly over the position of the embedded shell nodes k or directly over the shell quadrature points. the shell loads with respect to the Cartesian axes are given by:

$$q_{kj} = [-\tau_{jl}n_l - pn_l]_{Pf_k}, \tag{54}$$

where the indexes j and l represent Cartesian direction and n_l is the l component form the normal vector to Γ_s.

5 NUMERICAL EXAMPLES

5.1 Inflatable tube

In order to compare the proposed coupling procedure to the ALE scheme, we propose a problem consisting on a elastic tube with length $L = 0.7m$ along the x axis, diameter $D = 0.12m$ and thickness $h = 0.0025$, with all the nodes of coordinate $x \leq 0.05\ m$ or $x \geq 0.65\ m$ completely clamped.

The tube contains an ideal gas at rest with density $\rho_f = 1.2kg/m^3$ pressure $p = 99kPa$ and specific heat ratio $\gamma = 1.4$. At left hand side enters a gas with $\rho_{fi} = 2kg/m^3$, $p_{fi} = 200kPa$, producing a shock wave. At all right hand side and along the tube walls an slip wall boundary condition is applied. This condition is kept constant until $t = 0.0025\ s$, when the input is closed and the boundary conditions are slip wall over all the boundary.

The tube is discretized by 760 elements and 3468 nodes (Fig. 5.1 and its material has Young's modulus $E = 10MPa$, Poison ratio $\nu = 0.4$ and specific mass $\rho_s = 470kg/m^3$

The fluid mesh where the tube is immersed is depicted on Fig. 5.1, whit 211585 elements and 38147 nodes. For the ALE case we employ a mesh approximately with the same element size.

Figure 8 presents a snapshot of pressure distribution and displacement for both ALE and immersed case at $t = 0.004s$, where it is possible to observe good similarity.

On Fig. 9, a comparison between the radial displacements at $x = 0.34m$ is done.
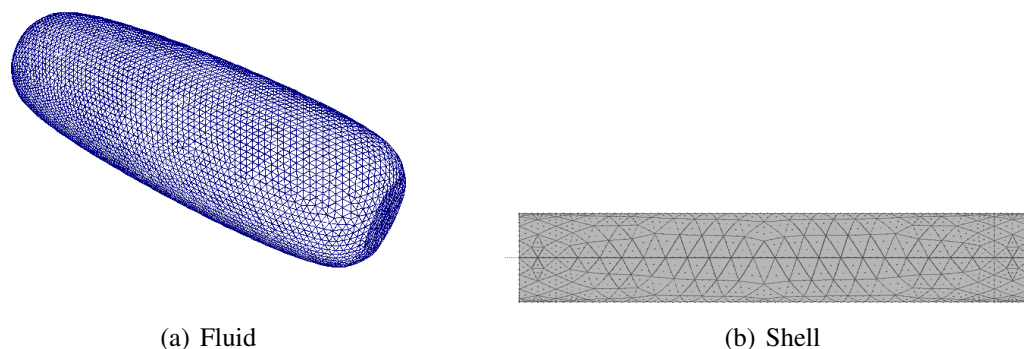

<center>(a) Fluid   (b) Shell</center>

<center>Figure 7: Tube discretization</center>

5.2 Airbag inflation

As a qualitative example, we simulate and airbag with the geometry given by Fig. 10.

(a) Immersed t = 0.001 s

(b) ALE t = 0.001 s

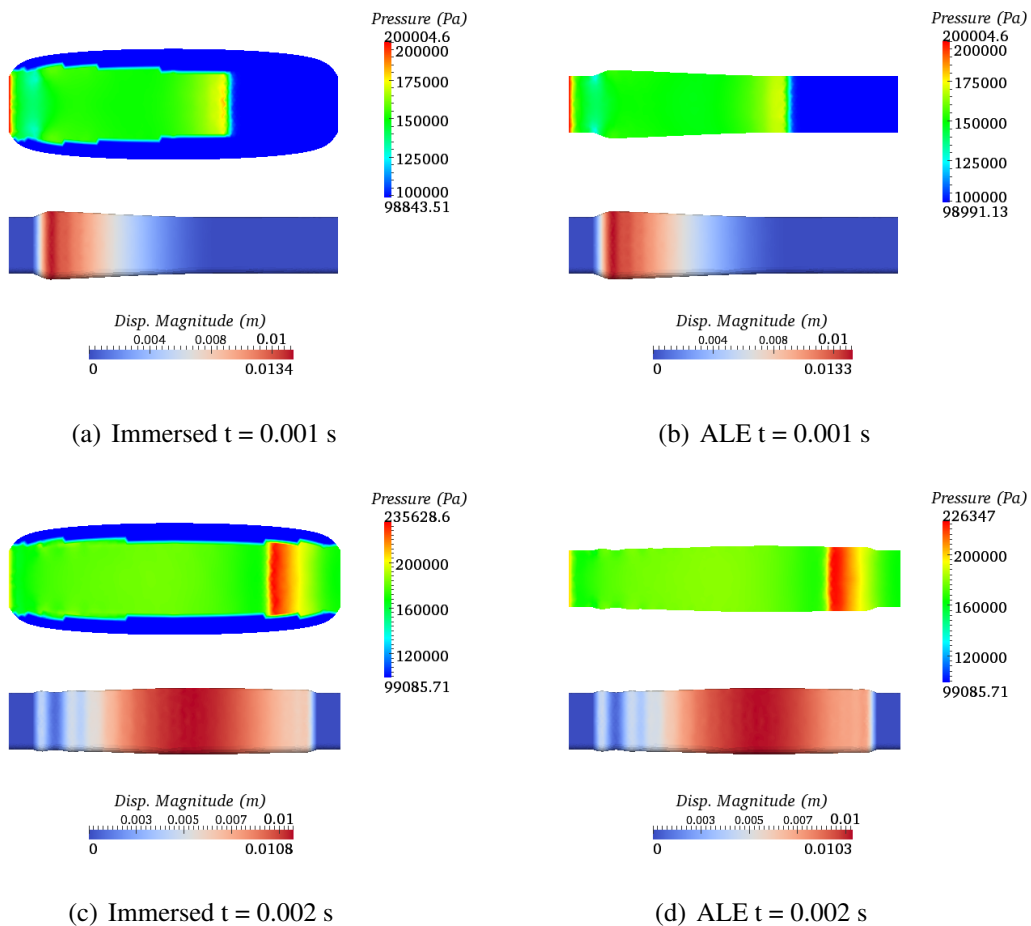(c) Immersed t = 0.002 s

(d) ALE t = 0.002 s

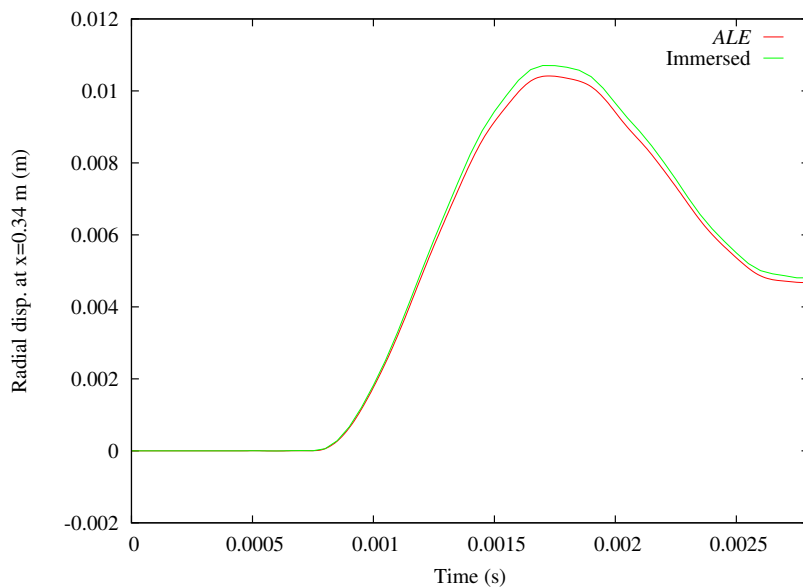Figure 8: Pressure distribution (Top) and shell displacements magnitude (Bottom)

Figure 9: Radial displacements vs. time at $x = 0.34$ m
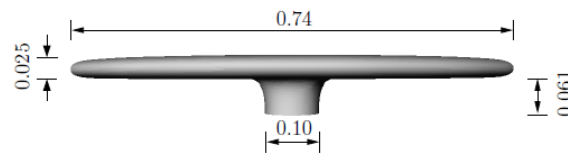
Figure 10: Airbag geometry adapted from Cirak and Radovitzky (2005)

This is only a qualitative example, once due to computational reasons the airbag mesh is not fine enough to represent the wrinkles that appears in high frequency and also the formulation is not ready to simulate self contact, what is common in a problem like this.

The airbag on its flat initial condition is filled with an ideal gas at rest with density $\rho_f = 1.3 kg/m^3$ pressure $p = 107 kPa$ and specific heat ratio $\gamma = 1.4$. At inlet enters a gas with $\rho_{fi} = 10 kg/m^3$, sound speed $c = 370 m/s$ and $\gamma = 1.4$ which produces a shock wave.

The input condition is kept constant until $t = 0.004\ s$, when the input is closed and the applied boundary condition is that of slip wall.

We assume that the problem is radially symmetric and discretize 1/4 of the problem. The airbag is discretized by 258 elements and 1237 nodes (Fig. 11(b) and its material has Young's modulus $E = 3GPa$ and specific mass $\rho_s = 1000 kg/m^3$ and thickness $h = 1.5mm$. The aibag is clamped over all the input area and simmetry boundary conditions are applied to the planes xz and yz.

The fluid mesh where the airbag is immersed is depicted on Fig. 11(a), whit 263667 elements and 47491 nodes.

Figure 12 presents a snapshots of pressure distribution and deformed airbag deformation at each $0.12ms$ and Fig. 13, plots the top displacement versus time.
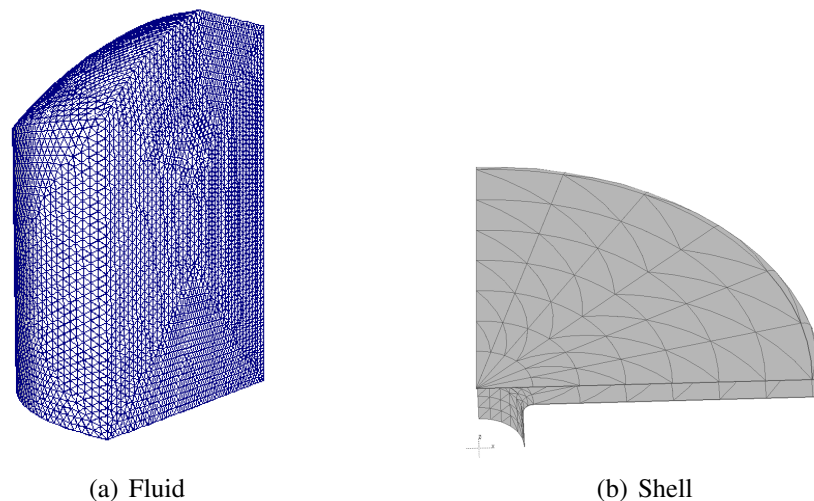

(a) Fluid   (b) Shell

Figure 11: Airbag discretization

These results show that the present procedure is a robust method for analysis of inflatable structures.

(a) t = 0.0012 s

(b) t = 0.0024 s

(c) t = 0.0036 s

(d) t = 0.0048 s
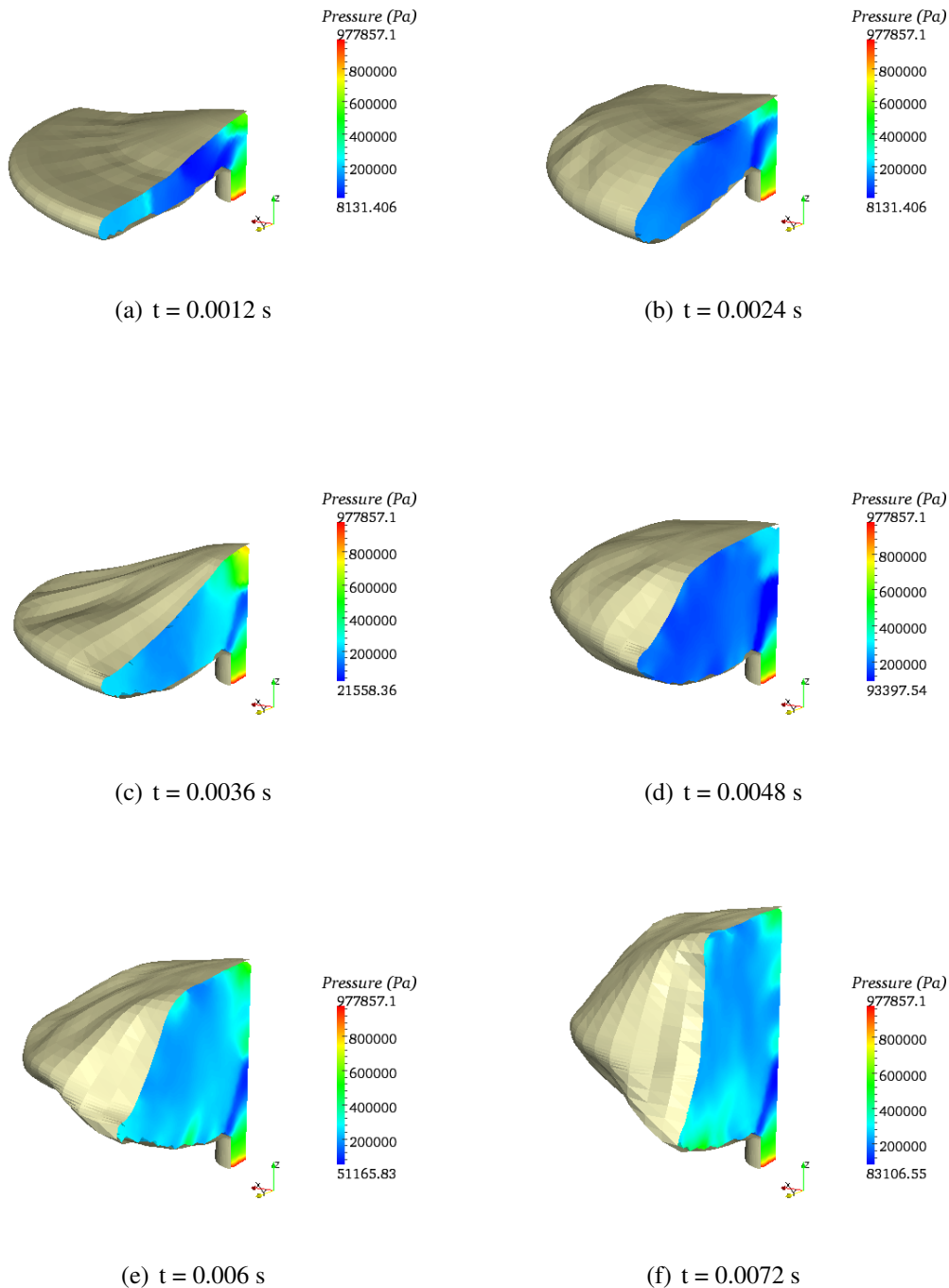
(e) t = 0.006 s

(f) t = 0.0072 s

Figure 12: Pressure snapshots

6 CONCLUSION

The proposed approach furnishes a general algorithm for explicit coupling of Lagrangian shell solvers with unstructured-mesh-based Eulerian fluid solvers.
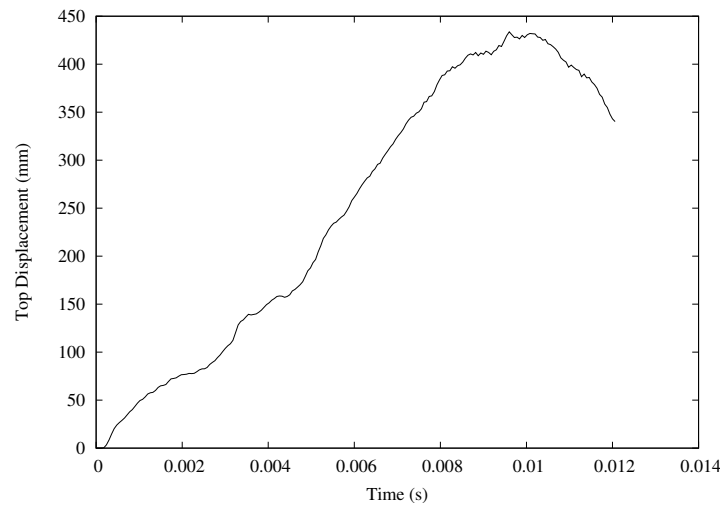
Figure 13: Top vertical displacements vs. time

Both, fluid and shell solver have demonstrated to be appropriate for fluid-structure analysis. The efficiency and robustness of the proposed approach is demonstrated with the inflatable structures examples.

For future works we suggest: 1. A complete quantitative numerical study. 2. A deep study of algorithms for signed distance function evaluation in order to optimize the computational performance. e. The extension of the fluid solver to incompressible flow cases. 4. The study of self impact models for the positional shell solver.

REFERENCES

Cirak F. and Radovitzky R. A lagrangian-eulerian shell-fluid coupling algorithm based on level sets. *Computers & Structures*, 83(6-7):491 – 498, 2005. ISSN 0045-7949. Frontier of Multi-Phase Flow Analysis and Fluid-Structure.

Coda H.B. and Paccola R.R. Unconstrained Finite Element for Geometrical Nonlinear Dynamics of Shells. *Mathematical problems in engineering*, 2009. ISSN 1024-123X.

Donea J., Giuliani S., and Halleux J.P. An arbitrary lagrangian-eulerian finite element method for transient dynamic fluid-structure interactions. *Computer Methods in Applied Mechanics and Engineering*, 33:689–723, 1982.

Fortuna O.A. *Técnicas computacionais para dinâmica dos fluidos*. EDUSP, São Paulo, Brasil, 2000.

Habbal F. *The Optimal Transportation Meshfree Method for General Fluid Flows and Strongly Coupled Fluid-Structure Interaction Problems*. Phd thesis, California Institute of Technology, Pasadena, California, 2009.

M. Arienti P. Hung E.M. and Shepherd J. A level set approach to eulerian-lagrangian coupling. *Caltech ASCI technical report 136*, 2008.

Nithiarasu P., Codina R., and Zienkiewicz O.C. The characteristic-based split (cbs) scheme - a unified approach to fluid dynamics. *International Journal for Numerical Methods in Engineering*, 66(10):1514–1546, 2006.

Ogden R. Non-linear elastic deformations. *Engineering Analysis*, 1(2):119 – 119, 1984. ISSN 0264-682X.

Sanches R.A.K. and Coda H.B. Formulação bidimensional alternativa para a interação fluido-

estrutura através do mef. In *XXIX Congresso Ibero Latino Americando de Métodos Computacionais em Engenharia - CILAMCE*. Maceió, Brazil, 2008.

Soria A. and Casadei F. Arbitrary Lagrangian-Eulerian multicomponent compressible flow with fluid-structure interaction. *International Journal for Numerical Methods in Fluids*, 25(11):1263–1284, 1997.

Teixeira P.R.F.E. and Awruch A.M. Numerical Simulation of fluid-structure interaction using the finite element method. *Computers and Fluids*, 34:249–273, 2005.

Valiappan S. *Continuum mechanics fundamentals*. A. A. BALKEMA, Rotterdam, 1981.

Zienkiewicz O.C. and Taylor R.L. *The Finite Element Method, v3: Fluid Dynamics*. Butterworth-heinemann Linacre house, 2000.